PAPER

Check for updates

Facile synthesis strategy for cesium tin halide perovskite crystals toward light emitting devices and anti-counterfeiting flexible fiber†

Ziyao Hu,[a] Kun Nie, [ID] *[a,b] Xuyi Wang,*[c] Xiuqiang Duan,[a] Ranran Zhou,[a] Mengyun Wu,[a] Xiaoxue Ma,*[a] Xiaodong Zhang,[a] Luoxin Wang,[a] Lefu Mei[d] and Hua Wang[a]

All-inorganic metal halide perovskites are widely studied because of their excellent photoelectric properties. However, due to the toxicity of $CsPbX_3$ (X = Cl, Br, I) perovskites, it is difficult to apply them on a large scale. The lead-free nature and air stability make Cs_2SnX_6 (X = Cl, Br, I) perovskites possible candidates to replace $CsPbX_3$ perovskites. Herein, we report the perovskite crystals (PCs) based on Te(IV)-doped Cs_2SnCl_6: $Cs_2Sn_{1-x}Te_xCl_6$. $Cs_2Sn_{1-x}Te_xCl_6$ PCs showed yellow emission under a 365 nm ultraviolet lamp. The photoluminescence quantum yield (PLQY) of $Cs_2Sn_{0.94}Te_{0.06}Cl_6$ PCs was 57.09%, which was proposed to be from the triplet Te(IV) ion $^3P_1 \rightarrow {}^1S_0$ self-trapping excitons (STE) recombination. The perovskite crystals can be used to fabricate light-emitting diodes (LEDs). The fiber paper prepared from aramid chopped fibers (ACFs) and polyphenylene sulfide (PPS) fibers showed a bright yellow light under 365 nm ultraviolet light after being post-processed with $Cs_2Sn_{1-x}Te_xCl_6$ PCs solution. The ACFs/PPS compound fiber paper modified with $Cs_2Sn_{1-x}Te_xCl_6$ PCs maintained exceptional optical properties and could be stored in air for more than 4500 h. The fluorescence performance of the modified ACFs/PPS compound fiber paper could be applied to fluorescence anti-counterfeiting. The modification strategy and the applications in this work will provide a good choice for studying the optical performance of perovskites and broaden the application of ACFs/PPS compound fiber paper.

Introduction

Lead halide $CsPbX_3$ (X = Cl, Br, I) perovskites are widely applied in optoelectronics because of their excellent optical performance.[1–3] For example, perovskites are widely used in photoelectric detection, solar cells, and other fields.[4–6] Perovskites are modified to improve their photoelectric conversion efficiency (PCE) and obtain the desired emission wavelength.[7–10] At the same time, the performance of perovskites can be improved by changing the morphologies of the perovskites.[11] The team of Miyasaka reported first metal halide perovskites solar cells with a PCE of 3.8%.[12] The PCE of perovskites solar cells is still rising.[13–15] However, the toxicity, and instability of lead-based perovskites make it difficult to use them in commercial applications.[16–18] The low toxicity and air stability of the element Sn(IV) make it possible for Cs_2SnX_6 (X = Cl, Br, I) to replace $CsPbX_3$.[19,20] However, although Cs_2SnCl_6 has a direct band gap, it hardly emits light under ultraviolet light. Therefore, synthesizing Cs_2SnCl_6 doped with other metal elements is of great significance to enhance its optical properties.

Doping refers to introducing impurities into intrinsic semiconductors to change their electrical properties.[21] Existing studies have shown that doping has an important effect on improving the optical performance of perovskites.[22] For instance, doping lanthanide into perovskite nanocrystals can greatly improve and expand the optical properties.[23] Sb-doped Cs_2SnCl_6 shows a photoluminescence peak at 630 nm with orange-red emission, and Bi-doped Cs_2SnCl_6 can yield blue self-trapping excitons (STE) emission. However, the unequal valence states between Bi^{3+} and Sn^{4+} make a large number of

[a]Hubei Key Laboratory for New Textile Materials and Applications and State Key Laboratory of New Textile Materials & Advanced Processing Technology, School of Materials Science and Engineering, Wuhan Textile University, Wuhan 430200, P. R. China. E-mail: knie@wtu.edu.cn, xxma@wtu.edu.cn
[b]Key Laboratory of Testing and Tracing of Rare Earth Products for State Market Regulation, Jiangxi University of Science and Technology, Ganzhou 341000, P. R. China
[c]China Bluestar Chengrand Co., Ltd, High Tech Organic Fiber Key Laboratory of Sichuan Province, Chengdu 610042, P. R. China. E-mail: xuyiwang2015@163.com
[d]Beijing Key Laboratory of Materials Utilization of Nonmetallic Minerals and Solid Wastes, National Laboratory of Mineral Materials, School of Materials Science and Technology, China University of Geosciences (Beijing), Beijing 100083, P. R. China
†Electronic supplementary information (ESI) available. See DOI: https://doi.org/10.1039/d3nr00301a

anion sublattices easily appear in the double-doped Cs_2SnCl_6, which may reduce the photoluminescence quantum yield (PLQY).[24] According to this view, tetravalent ion doping can significantly reduce the formation of extrinsic defects and promote optical properties. A lead-free perovskite $Cs_2Sn_{1-x}Te_xCl_6$ can show a bright yellow light under the irradiation of 365 nm ultraviolet light and has high anti-water stability.[25] A Te^{4+}-doped Cs_2SnCl_6 vacancy-ordered perovskite variant shows green-yellow emission.[26] However, the previous synthesis methods required some special ligands or Teflon liners. Therefore, it is urgent to synthesize $Cs_2Sn_{1-x}Te_xCl_6$ using a more economical and convenient method. In this paper, $Cs_2Sn_{1-x}Te_xCl_6$ perovskite crystals (PCs) with different doping ratios were synthesized *via* a more convenient hydrothermal method. A light-emitting diode (LED) lamp was fabricated by combining a 385 nm chip and $Cs_2Sn_{0.94}Te_{0.06}Cl_6$ PCs. The LED lamp could emit yellow light driven by a 600 mA current. Furthermore, we have modified fiber paper prepared from aramid chopped fibers (ACFs) and polyphenylene sulfide (PPS) fiber by post-processing it with the $Cs_2Sn_{1-x}Te_xCl_6$ PCs solution. The modified ACFs/PPS compound fiber paper showed a bright yellow light under 365 nm ultraviolet light. The modified fiber paper could maintain exceptional optical properties even when soaked in a weak acid solution (pH = 5). The optical properties of the modified ACFs/PPS compound fiber paper can be applied in fluorescence anti-counterfeiting. The modification strategy and the application in this paper will provide a good choice for studying the optical properties of perovskites and broaden the application of ACFs/PPS compound fiber paper.

Results and discussion

$Cs_2Sn_{1-x}Te_xCl_6$ PCs with different doping ratios were synthesized *via* a more convenient hydrothermal method (shown in Fig. 1b). The ACFs/PPS compound fiber paper was prepared *via* a wet papermaking method (shown in Fig. 1c). The left part of Fig. 1a shows the crystal structure of Cs_2SnCl_6. Tetravalent

tin(IV) ions usually occupy the central site and form the standalone $[SnCl_6]^{2-}$ octahedral structure. The crystal structure of $Cs_2Sn_{1-x}Te_xCl_6$ is shown in the right part of Fig. 1a. The $[TeCl_6]^{2-}$ replaced part of the $[SnCl_6]^{2-}$ by doping with tetravalent Te(IV). The X-ray diffraction (XRD) patterns and photoluminescence (PL) spectra of $Cs_2Sn_{0.94}Te_{0.06}Cl_6$ with different reaction times are shown in Fig. S1 and S2.† The PL intensity of the $Cs_2Sn_{0.94}Te_{0.06}Cl_6$ PCs obtained after 60 minutes of reaction is the highest. The XRD pattern of un-doped Cs_2SnCl_6 matches well with the standard card (no.: 07-0197) (Fig. 2a). There were no impurity diffraction peaks observed after doping Te^{4+} into Cs_2SnCl_6 because of the similar coordination property to halogen of elements Te and Sn,[26] which proved that the synthesized $Cs_2Sn_{1-x}Te_xCl_6$ perovskite crystals were of high purity. At the same time, the optical properties (shown in Fig. 4(a)) of the doped perovskite crystals have been significantly improved. It can be reasonably inferred that part of $[TeCl_6]^{2-}$ replaces $[SnCl_6]^{2-}$ in the structure. The X-ray photoelectron spectroscopy XPS spectra (Fig. 2b) showed the specific elements' content of Cs_2SnCl_6 and $Cs_2Sn_{0.94}Te_{0.06}Cl_6$. The detailed XPS spectra (Fig. 2c, d, and f) of Cs, Sn, and Cl of $Cs_2Sn_{0.94}Te_{0.06}Cl_6$ were practically consistent with Cs_2SnCl_6. In contrast, the XPS spectrum of Te of $Cs_2Sn_{0.94}Te_{0.06}Cl_6$ was different from that of Cs_2SnCl_6, which proved that Te had been doped into Cs_2SnCl_6 successfully. The atomic ratio of Cs, Sn, and Cl in un-doped Cs_2SnCl_6 was close to 2 : 1 : 6. The atomic ratio of Te in $Cs_2Sn_{1-x}Te_xCl_6$ increased with the doping concentration increasing (shown in Table S1†). The scanning electron microscope (SEM) image of un-doped Cs_2SnCl_6 is shown in Fig. 3a. The elemental mapping images of Cs, Sn, Te, and Cl in $Cs_2Sn_{0.94}Te_{0.06}Cl_6$ are shown in Fig. 3b–f. The SEM image of $Cs_2Sn_{0.94}Te_{0.06}Cl_6$ is shown in Fig. 3g. It can be observed that the crystal morphology of $Cs_2Sn_{1-x}Te_xCl_6$ after modification is almost unchanged.

The PL and photoluminescence excitation (PLE) spectra of $Cs_2Sn_{1-x}Te_xCl_6$ PCs are shown in Fig. 4a and b. The un-doped Cs_2SnCl_6 was hardly luminous, while the PL intensities of $Cs_2Sn_{1-x}Te_xCl_6$ were significantly enhanced. It could be observed that the PL intensity of $Cs_2Sn_{1-x}Te_xCl_6$ was the highest when $x = 0.06$ and then decreased with the increase in Te^{4+} doping. According to previous reports, this reduction in PL was attributed to the concentration quenching process where the excitation energy migrated to the quenching sites through the lattice.[27] They calculated the critical distance (R) for $[TeCl_6]^{2-}$–$[TeCl_6]^{2-}$ energy transfer. According to the formula $R^6 = (0.6 \times 10^{28})(4.8 \times 10^{-16} f/E^4)SO$, the calculated R is almost three times the shortest Te–Te distance, which means that there is the possibility of energy transfer. f is the oscillator strength of the relevant $^1S_0 \rightarrow {}^3P_1$ transition and is taken to be 10^{-2}; E, the energy of maximum spectral overlap, is 2.5 eV; SO, the spectral overlap of emission and absorption, amounts to 0.1 eV^{-1}. The peak position of the PL intensity showed a slight red shift with the increase in the amount of Te^{4+} doped. For halide perovskites with a soft lattice, the photogenerated electrons at the excited state levels tend to be coupled with lattice vibration, causing transient lattice distortion, changing
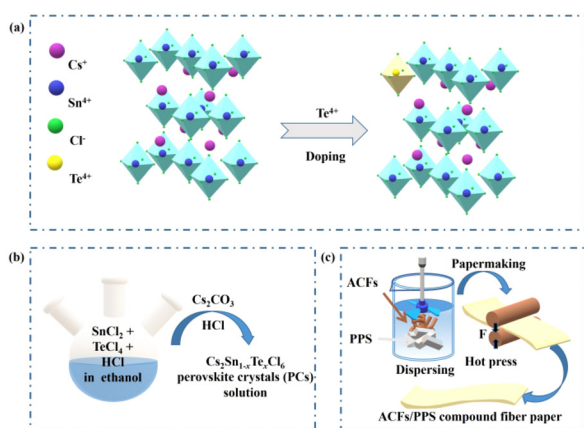

Fig. 1 (a) The crystal structures of Cs_2SnCl_6 and $Cs_2Sn_{1-x}Te_xCl_6$ perovskite crystals. (b) and (c) Schematic diagrams of the synthesis of $Cs_2Sn_{1-x}Te_xCl_6$ perovskite crystals and ACFs/PPS compound fiber paper.

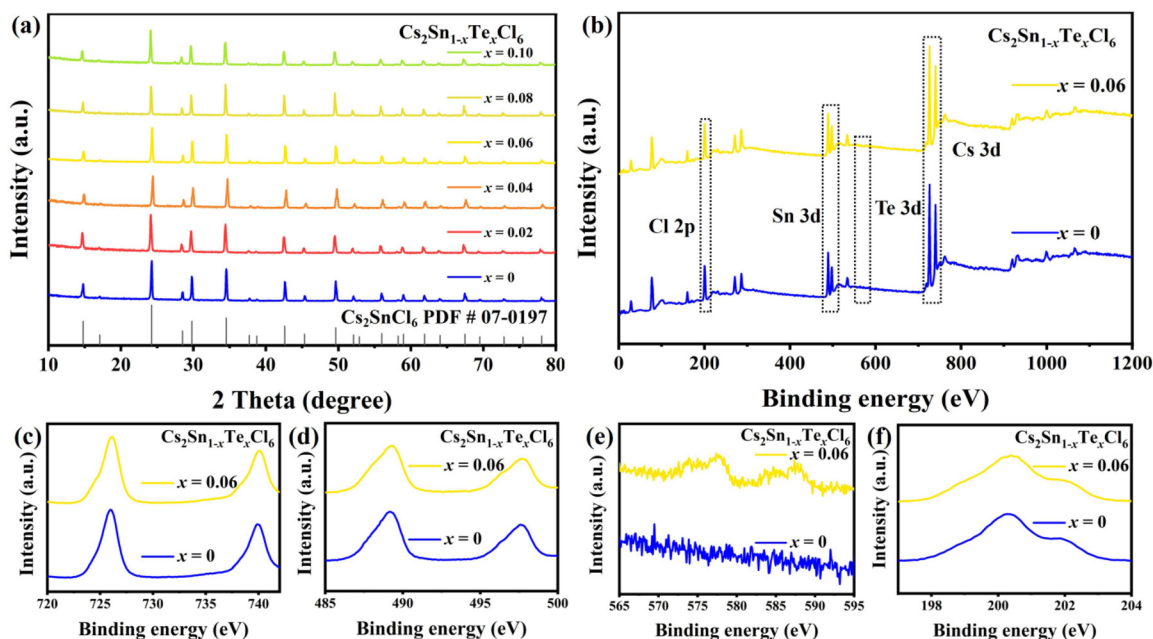**Fig. 2** (a) XRD patterns of Cs_2SnCl_6 and $Cs_2Sn_{1-x}Te_xCl_6$ (x = 0.02, 0.04, 0.06, 0.08, 0.10) perovskite crystals. The bottom pattern is the standard card of Cs_2SnCl_6. (b) XPS spectra of Cs_2SnCl_6 and $Cs_2Sn_{0.94}Te_{0.06}Cl_6$. (c–f) XPS spectra of Cs_2SnCl_6 and $Cs_2Sn_{0.94}Te_{0.06}Cl_6$ clearly show the Cs, Sn, Te, and Cl elements.

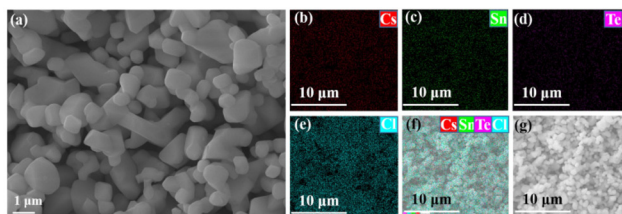**Fig. 3** (a) SEM image of Cs_2SnCl_6. (b–f) Elemental mapping images of Cs, Sn, Te, Cl in $Cs_2Sn_{0.94}Te_{0.06}Cl_6$. (g) SEM image of $Cs_2Sn_{0.94}Te_{0.06}Cl_6$.

nuclear coordinates, and producing local STE.[28] Tetravalent Te, as a typical ion with the outer electronic configuration of $5s^2$, has five energy levels: ground state of $^1S_0$ and singlet/triplet excited states of $^1P_1/^3P_n$ (n = 0, 1, 2).[29] Self-trapping excitons widely exist in perovskites.[30] In some perovskite crystals, the electrons and holes generated by excitation will immediately be self-trapped because the self-trapped state is more stable. According to other reports, both a broad PL band and large Stokes shift are typical features of STE emission.[31,32] Take $Cs_2Sn_{0.94}Te_{0.06}Cl_6$ for example, the PL band starts at 450 nm and ends at 700 nm. The excitation wavelength is 385 nm, and the emission wavelength is 553 nm. Based on these data, it can be reasonably inferred that the fluorescence property of Te-doped Cs_2SnCl_6 is due to STE emission. Fig. 4c and d are the PL and PLE spectra of $Cs_2Sn_{0.94}Te_{0.06}Cl_6$ PCs. It can be observed that the PL and PLE spectra almost maintain the same wave profile no matter how the excitation and emission change, which proves that the emission band is the luminescence characteristic of $Cs_2Sn_{0.94}Te_{0.06}Cl_6$ PCs, not the surface defects or the lattice defects of the samples. The test

results verify the STE and ion luminescence characteristics of $Cs_2Sn_{1-x}Te_xCl_6$. Fig. 4e and f are the two-dimensional (2D) and three-dimensional (3D) fluorescence spectra of $Cs_2Sn_{0.94}Te_{0.06}Cl_6$ PCs. It can be observed that the emission wavelength varies between 500 nm to 600 nm, while the excitation wavelength varies between 250 nm to 450 nm. The time-resolved (TRPL) decay curves (shown in Fig. 5a) of $Cs_2Sn_{1-x}Te_xCl_6$ PCs can be well fitted with the bi-exponential eqn (1):[33]

$$I(t) = A_1 \exp(-t/\tau_1) + A_2 \exp(-t/\tau_2). \qquad (1)$$

The average fluorescence lifetime can be calculated using eqn (2):[21]

$$\tau_{avg} = (A_1\tau_1{}^2 + A_2\tau_2{}^2)/(A_1\tau_1 + A_2\tau_2). \qquad (2)$$

It can be calculated that the average fluorescence lifetimes of $Cs_2Sn_{1-x}Te_xCl_6$ PCs are 2.06 μs (x = 0.02), 38.61 μs (x = 0.06) and 1.83 μs (x = 0.08). At the same time, combined with the PL spectra (Fig. 4(a)), the emission intensity of the sample is positively related to its lifetime. The chromaticity coordinate (CIE) values of un-doped Cs_2SnCl_6 PCs and $Cs_2Sn_{1-x}Te_xCl_6$ can be calculated to be (0.23, 0.21), (0.38, 0.52), (0.39, 0.54), (0.39, 0.55), (0.39, 0.54), (0.38, 0.53), which appeared in the yellow area of the CIE (Fig. 5b). The color purity of $Cs_2Sn_{1-x}Te_xCl_6$ PCs can be calculated from eqn (3):[34]

$$\text{Color purity} = \sqrt{\frac{(x - x_i)^2 + (y - y_i)^2}{(x_d - x_i)^2 + (y_d - y_i)^2}} \times 100\% \qquad (3)$$

(x, y), (x_i, y_i), and (x_d, y_d) conform to the CIE color coordinates of the $Cs_2Sn_{1-x}Te_xCl_6$ PCs, white light illumination, and domi-
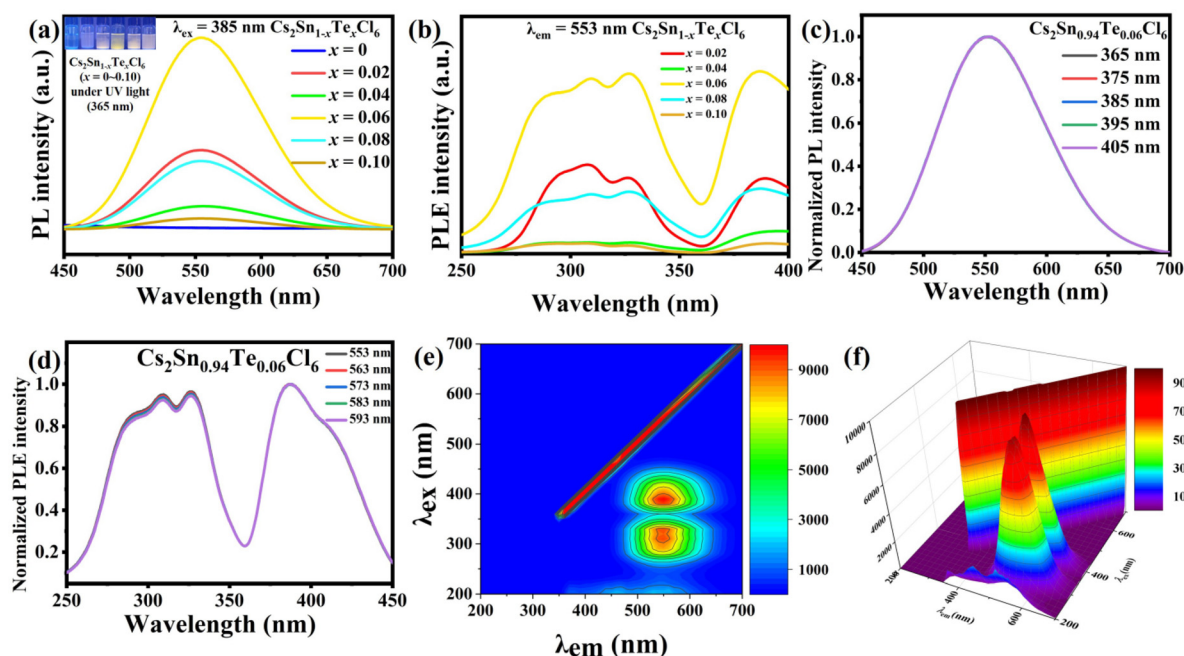
Fig. 4 (a) PL spectra of Cs_2SnCl_6 and $Cs_2Sn_{1-x}Te_xCl_6$ (x = 0.02, 0.04, 0.06, 0.08, 0.10) PCs. (b) PLE spectra of $Cs_2Sn_{1-x}Te_xCl_6$ (x = 0.02, 0.04, 0.06, 0.08, 0.10) PCs. (c) PL spectra of $Cs_2Sn_{0.94}Te_{0.06}Cl_6$ PCs with different excitation wavelengths. (d) PLE spectra of $Cs_2Sn_{0.94}Te_{0.06}Cl_6$ PCs under the different monitoring wavelengths. (e) and (f) 2D and 3D wavelength scanning spectra of $Cs_2Sn_{0.94}Te_{0.06}Cl_6$.
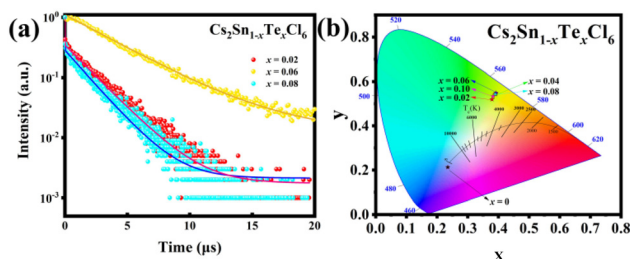

Fig. 5 (a) TRPL decay curves of $Cs_2Sn_{1-x}Te_xCl_6$ (x = 0.02, 0.06, 0.08) PCs. (b) Chromaticity coordinates (CIE 1931) of $Cs_2Sn_{1-x}Te_xCl_6$ (x = 0.02, 0.04, 0.06, 0.08, 0.10) PCs.

nant wavelength, respectively. For $Cs_2Sn_{0.94}Te_{0.06}Cl_6$ PCs, the concrete values of (x, y), (x_i, y_i), and (x_d, y_d) are (0.39, 0.55), (0.33, 0.33), (0.40, 0.59). It can be calculated that the color purity of $Cs_2Sn_{0.94}Te_{0.06}Cl_6$ PCs is 84.69%. The color purity of the sample indicated that it had the potential to manufacture LED lamps for general lighting. To further test and verify the application of $Cs_2Sn_{1-x}Te_xCl_6$ PCs for LEDs, a LED lamp was fabricated by combining the 385 nm n-UV chip and $Cs_2Sn_{0.94}Te_{0.06}Cl_6$ PCs. The electroluminescence (EL) spectrum of this LED lamp driven by the current is shown in Fig. 6e. The driving current is 600 mA and the corresponding output power is 3 W. The LED lamp produces CIE (shown in Fig. S3†) color coordinates of (0.35, 0.37) with a correlated color temperature (CCT) of 4879 K, which shows that $Cs_2Sn_{0.94}Te_{0.06}Cl_6$ perovskite crystals have potential in the manufacture of LED lamps for general lighting.

Meanwhile, we modified the ACFs/PPS compound fiber paper by post-processing it with $Cs_2Sn_{0.94}Te_{0.06}Cl_6$ PCs solution. Fig. 6a shows that the modified ACFs/PPS compound fiber paper showed bright yellow light under UV light while the unmodified paper did not. Although stored in air for more than 4500 h, the modified fiber paper still showed a bright yellow light (Fig. 6b). Furthermore, the modified paper can still maintain luminescence characteristics when it was immersed in a weak acid solution (Fig. 6f). The PLQY of the modified fiber paper soaked in a weak acid solution was 17.63%. It could be observed that the fluorescence intensities of the modified fiber paper decreased with the increase in temperature (Fig. 6c). It was similar to the reduction in PL intensity due to the participation of phonons in nonradiative recombination at high temperatures. The thermal stability of the modified ACFs/PPS compound fiber paper can be verified by the thermogravimetric analysis (Fig. 6d). PL spectra of the ACFs/PPS composite fiber paper were measured at 50 °C and after falling back from 250 °C (shown in Fig. S4(a)†). The modified composite fiber paper could retain 82% of the original emission intensity when it fell from 250 to 50 °C. In addition, PL intensities of the ACFs/PPS composite fiber paper were measured at different temperatures. The intensity of PL decreased gradually with increasing temperature (shown in Fig. S4(b)†). However, after heating for 5 min, an enhancement in the PL intensity at some temperatures can be seen. Furthermore, the average intensity of PL can still maintain 98% of the original PL intensity when it falls from 100 to 40 °C. It can be observed that the sublimation temperature of the modified ACFs/PPS compound fiber paper is about 300 °C
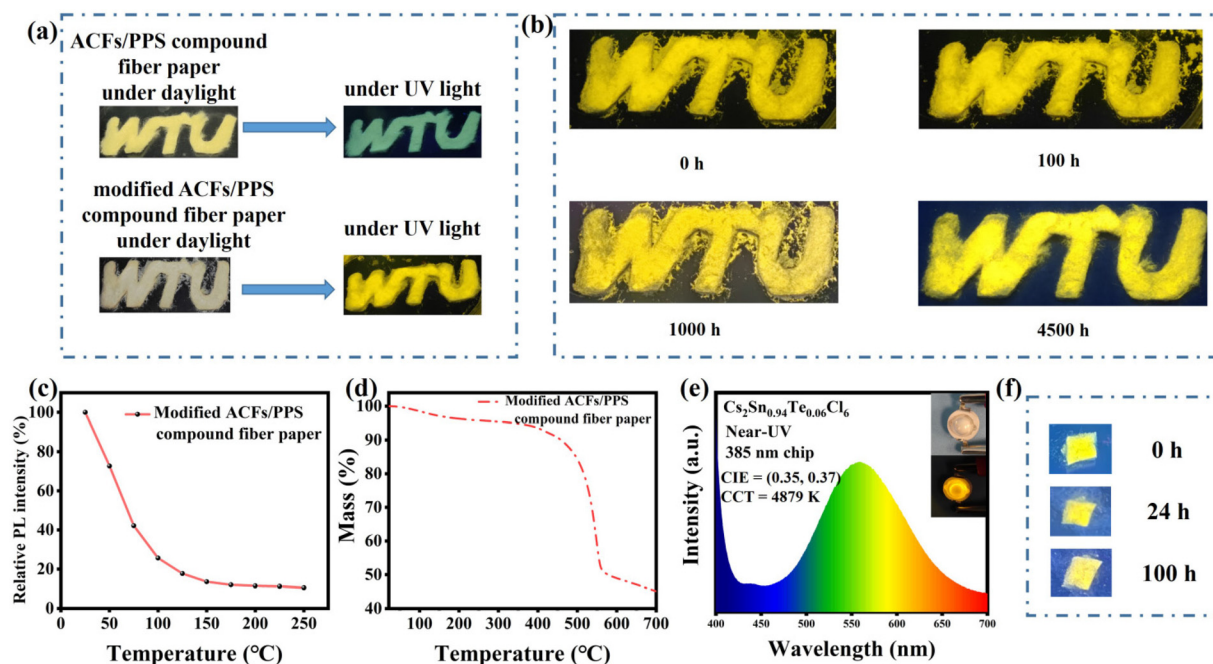
Fig. 6 (a) Fluorescent properties of ACFs/PPS compound fiber paper without modification and modified with $Cs_2Sn_{0.94}Te_{0.06}Cl_6$ PCs solution. (b) The stability of modified ACFs/PPS compound fiber paper in air. (c) The relative PL spectrum of modified ACFs/PPS compound fiber paper at different temperatures. (d) TGA of modified ACFs/PPS compound fiber paper. (e) Electroluminescence spectrum of light-emitting diode (LED) lamp fabricated *via* the combination of a near-ultraviolet 385 nm n-UV chip and $Cs_2Sn_{0.94}Te_{0.06}Cl_6$ perovskite crystals. (Inset) Digital images of the LED package with and without current input. (f) Fluorescent properties of modified ACFs/PPS compound fiber paper in weak acid solution.

(Fig. 6c). Based on the above data, it can be concluded that the ACFs/PPS composite fiber paper has a certain degree of thermal stability. These test results have laid a good foundation for use of the modified ACFs/PPS compound fiber paper as a fluorescent anti-counterfeiting material.

Conclusions

To sum up, the $Cs_2Sn_{1-x}Te_xCl_6$ PCs were synthesized *via* a more convenient hydrothermal method. The synthesized perovskite crystals showed obvious fluorescence and the emission center was 553 nm. $Cs_2Sn_{0.94}Te_{0.06}Cl_6$ PCs showed the highest fluorescence intensity, where the PLQY could reach 57.09%. Through the PL and PLE spectra, it could be inferred that the fluorescence of $Cs_2Sn_{1-x}Te_xCl_6$ PCs was attributed to the doping of the Te element. The LED lamp fabricated by combining a 385 nm n-UV chip and $Cs_2Sn_{0.94}Te_{0.06}Cl_6$ PCs could emit yellow light driven by the current. Furthermore, ACFs/PPS compound fiber paper was post-processed with $Cs_2Sn_{1-x}Te_xCl_6$ PCs solution. The test results in this paper showed that the modified ACFs/PPS compound fiber paper can maintain fluorescence properties in air and a weak acid environment for a long time, which laid a good foundation for it as a fluorescent anti-counterfeiting material. This work provides a good choice to study the optical performance of perovskites crystals and broadens the application of the ACFs/PPS compound fiber paper.

Author contributions

Ziyao Hu: conceptualization, investigation, methodology, data curation, formal analysis, writing – original draft; Kun Nie: resources, conceptualization, supervision, project administration, funding acquisition, writing – review and editing; Xuyi Wang: project administration, funding acquisition; Xiuqiang Duan: investigation, methodology; Ranran Zhou: investigation, methodology; Mengyun Wu: investigation; Xiaoxue Ma: resources; Xiaodong Zhang: investigation; Luoxin Wang: project administration, funding acquisition; Lefu Mei: funding acquisition, project administration; Hua Wang: funding acquisition, project administration.

Conflicts of interest

There are no conflicts to declare.

Acknowledgements

Notes and references

1 L. Protesescu, S. Yakunin, M. I. Bodnarchuk, F. Krieg, R. Caputo, C. H. Hendon, R. X. Yang, A. Walsh and M. V. Kovalenko, *Nano Lett.*, 2015, **15**, 3692–3696.

2 G. Nedelcu, L. Protesescu, S. Yakunin, M. I. Bodnarchuk, M. J. Grotevent and M. V. Kovalenko, *Nano Lett.*, 2015, **15**, 5635–5640.

3 J. Song, J. Li, X. Li, L. Xu, Y. Dong and H. Zeng, *Adv. Mater.*, 2015, **27**, 7162–7167.

4 J. Deng, J. Li, Z. Yang and M. Wang, *J. Mater. Chem. C*, 2019, **7**, 12415–12440.

5 F. Wang, M. Endo, S. Mouri, Y. Miyauchi, Y. Ohno, A. Wakamiya, Y. Murata and K. Matsuda, *Nanoscale*, 2016, **8**, 11882–11888.

6 L. Y. Wang, L. L. Deng, X. Wang, T. Wang, H. R. Liu, S. M. Dai, Z. Xing, S. Y. Xie, R. B. Huang and L. S. Zheng, *Nanoscale*, 2017, **9**, 17893–17901.

7 K. A. Bush, A. F. Palmstrom, Z. J. Yu, M. Boccard, R. Cheacharoen, J. P. Mailoa, D. P. McMeekin, R. L. Z. Hoye, C. D. Bailie, T. Leijtens, I. M. Peters, M. C. Minichetti, N. Rolston, R. Prasanna, S. Sofia, D. Harwood, W. Ma, F. Moghadam, H. J. Snaith, T. Buonassisi, Z. C. Holman, S. F. Bent and M. D. McGehee, *Nat. Energy*, 2017, **2**, 17009.

8 M. Jiang, J. Yuan, G. Cao and J. Tian, *Chem. Eng. J.*, 2020, **402**, 126152.

9 M. I. Kholil and M. T. Hossen Bhuiyan, *RSC Adv.*, 2020, **10**, 43660–43669.

10 Y.-H. Song, J. S. Yoo, E. K. Ji, C. W. Lee, G. S. Han, H. S. Jung and D.-H. Yoon, *Chem. Eng. J.*, 2016, **306**, 791–795.

11 R. Zhou, C. A. Cheng, S. Qiu, J. Chen, K. Nie, M. Wu, P. Lin, H. Wang, L. Wang and L. Mei, *RSC Adv.*, 2021, **11**, 28716–28722.

12 A. Kojima, K. Teshima, Y. Shirai and T. Miyasaka, *J. Am. Chem. Soc.*, 2009, **131**, 6050–6051.

13 S. S. Mali, C. S. Shim, H. Kim, P. S. Patil and C. K. Hong, *Nanoscale*, 2016, **8**, 2664–2677.

14 Y. Liu, W. Xiang, S. Mou, H. Zhang and S. Liu, *Chem. Eng. J.*, 2022, **447**, 137515.

15 N.-G. Park, *Mater. Today*, 2015, **18**, 65–72.

16 A. Babayigit, A. Ethirajan, M. Muller and B. Conings, *Nat. Mater.*, 2016, **15**, 247–251.

17 W. Ke and M. G. Kanatzidis, *Nat. Commun.*, 2019, **10**, 965.

18 A. H. Slavney, R. W. Smaha, I. C. Smith, A. Jaffe, D. Umeyama and H. I. Karunadasa, *Inorg. Chem.*, 2017, **56**, 46–55.

19 T. C. Jellicoe, J. M. Richter, H. F. Glass, M. Tabachnyk, R. Brady, S. E. Dutton, A. Rao, R. H. Friend, D. Credgington, N. C. Greenham and M. L. Bohm, *J. Am. Chem. Soc.*, 2016, **138**, 2941–2944.

20 X. Qiu, B. Cao, S. Yuan, X. Chen, Z. Qiu, Y. Jiang, Q. Ye, H. Wang, H. Zeng, J. Liu and M. G. Kanatzidis, *Sol. Energy Mater. Sol. Cells*, 2017, **159**, 227–234.

21 J. Jiang, Q. Wang, Z. Jin, X. Zhang, J. Lei, H. Bin, Z.-G. Zhang, Y. Li and S. F. Liu, *Adv. Energy Mater.*, 2018, **8**, 1701757.

22 W. J. Mir, Y. Mahor, A. Lohar, M. Jagadeeswararao, S. Das, S. Mahamuni and A. Nag, *Chem. Mater.*, 2018, **30**, 8170–8178.

23 G. Pan, X. Bai, D. Yang, X. Chen, P. Jing, S. Qu, L. Zhang, D. Zhou, J. Zhu, W. Xu, B. Dong and H. Song, *Nano Lett.*, 2017, **17**, 8005–8011.

24 A. Yan, K. Li, Y. Zhou, Y. Ye, X. Zhao and C. Liu, *J. Alloys Compd.*, 2020, **822**, 153528.

25 Z. Tan, Y. Chu, J. Chen, J. Li, G. Ji, G. Niu, L. Gao, Z. Xiao and J. Tang, *Adv. Mater.*, 2020, **32**, 2002443.

26 R. Zeng, K. Bai, Q. Wei, T. Chang, J. Yan, B. Ke, J. Huang, L. Wang, W. Zhou, S. Cao, J. Zhao and B. Zou, *Nano Res.*, 2021, **14**, 1551–1558.

27 G. Blasse, G. J. Dirksen and W. Abriel, *Chem. Phys. Lett.*, 1987, **136**, 460–464.

28 B. Ke, R. Zeng, Z. Zhao, Q. Wei, X. Xue, K. Bai, C. Cai, W. Zhou, Z. Xia and B. Zou, *J. Phys. Chem. Lett.*, 2020, **11**, 340–348.

29 T. V. Sedakova and A. G. Mirochnik, *Opt. Spectrosc.*, 2016, **120**, 268–273.

30 S. You, T. Zhu, Y. Wang, Z. K. Zhu, Z. Li, J. Wu, P. Yu, L. Li, C. Ji, Y. Wang, S. Wang and J. Luo, *Adv. Funct. Mater.*, 2022, 2210481.

31 B. M. Benin, D. N. Dirin, V. Morad, M. Worle, S. Yakunin, G. Raino, O. Nazarenko, M. Fischer, I. Infante and M. V. Kovalenko, *Angew. Chem., Int. Ed.*, 2018, **57**, 11329–11333.

32 V. Morad, Y. Shynkarenko, S. Yakunin, A. Brumberg, R. D. Schaller and M. V. Kovalenko, *J. Am. Chem. Soc.*, 2019, **141**, 9764–9768.

33 R. Zhou, C. A. Cheng, X. Wang, K. Nie, J. Wu, M. Wu, X. Duan, Z. Hu, I. U. Huq, H. Wang, L. Wang, L. Mei, H. Liu and X. Ma, *Nano Res.*, 2023, **16**, 3542–3551.

34 K. Nie, X. Ma, P. Lin, N. Kumar, L. Wang and L. Mei, *J. Rare Earths*, 2021, **39**, 1320–1326.